Cluster formation in sputtering: A molecular dynamics study using the MD/MC-corrected effective medium potential

A. Wucher[a)]
Fachbereich Physik, University of Kaiserslautern, 67653 Kaiserslautern, Germany

B. J. Garrison
Department of Chemistry, Pennsylvania State University, University Park, Pennsylvania 16802

(Received 4 April 1996; accepted 25 June 1996)

We report on a molecular dynamics simulation of cluster emission during sputtering of metals using a new many-body potential developed by DePristo and co-workers. For the specific case of silver as a sample target material, it is shown that this potential allows a much more realistic description of small clusters than the EAM potential used in our previous work. While this has a relatively large effect on the relative abundance of clusters within the total flux of sputtered material, other cluster properties like kinetic energy distributions and internal excitation are found to be less affected. By comparison with corresponding experimental data, we conclude that the formation of sputtered silver clusters can now be almost quantitatively modeled by the simulation. © *1996 American Institute of Physics.* [S0021-9606(96)01737-0]

I. INTRODUCTION

The theoretical description of cluster formation during sputtering of solids has been a challenging problem in sputtering physics for more than two decades. For a review of the relatively large amount of related work, which has appeared in the literature, the reader is referred to the fairly recent review by Urbassek and Hofer.[1] Among the different basic approaches used to model the emission and/or formation of sputtered clusters, computer simulation using molecular dynamics (MD) seems to be one of the most promising tools to describe the multiple many-body collision processes which lead to the emission of a cluster. In MD, the atomic motions of all atoms in a model crystal are followed simultaneously. The method therefore automatically delivers the spatial and temporal correlation between sputtered atoms which is of great importance for cluster emission phenomena in sputtering. In addition, the smooth variation of the potential governing the interaction between sputtered atoms (which may eventually form a cluster) on their way from a solid to a gas phase environment far away from the surface can in a natural way be reproduced by MD, provided the functional form of the interaction potential used in the simulation allows the simultaneous and realistic description of a solid and small gas phase clusters. After the early pioneering work, in which pairwise additive potentials were exclusively employed,[2–10] a number of MD studies of cluster sputtering have recently been performed[11–22] using many-body interaction potentials which, for the case of metals, were constructed by the so-called embedded-atom method (EAM).[23] Here, the potential is parametrized in a relatively simple functional form, the parameters of which are fit to reproduce the main properties of the respective solid material. Our previous study on silver clusters as a model system, however, revealed that the EAM potential fit for silver significantly overbinds small Ag_n clusters.[12] The implication of this was not entirely clear at the time being; it was argued that the effect accounted for the significant overestimation of calculated cluster sputtering yields[12,15,17] with respect to corresponding experimental data,[24–27] while other properties of sputtered clusters—like kinetic energy or internal excitation—may not be influenced by the overboundedness as much. The latter assumption, however, is not obvious since it was found that unimolecular fragmentation of internally excited "nascent" clusters on their path away from the surface plays a strong role in the formation of experimentally detectable sputtered clusters.[12,15,28] The kinetics of such unimolecular reactions, on the other hand, are determined by the exact shape of the potential hypersurface and may therefore well be influenced by only moderate changes of the interaction potential. In the present work, we therefore repeat the MD simulation of silver cluster sputtering using a new many-body potential originally developed by DePristo and co-workers.[29] First, it will be shown that this potential, which is partially based on some experimental dimer data, allows a much more realistic description of small gas phase silver clusters than does the EAM potential used in our previous work. Then, basic properties like yields, kinetic, and internal energy distributions of nascent as well as experimentally detectable "final" clusters (i.e., clusters which represent the stable products of unimolecular fragmentation chains) will be calculated and compared to those predicted by the EAM potential as well as to available experimental data.

II. DESCRIPTION OF THE CALCULATION

The molecular dynamics simulation as well as its extension towards the formation and fragmentation of clusters in sputtering has been described in great detail earlier.[12,30] In short, the classical equations of motion are solved numerically for all atoms of a crystallite which in the present case contains ~2300 metal atoms. While the interaction between the impinging Ar^+ ion and the metal atoms was described by

[a)]Electronic mail: wucher@rhrk.uni-kl.de

 0021-9606/96/105(14)/5999/9/$10.00

a conventional pair potential of the Molière type,[30] a many-body potential originally designed by DePristo and co-workers[29,31] was used to describe the interaction between target atoms. The functional form of this potential, which has been termed "molecular dynamics and Monte Carlo-corrected effective medium" (MD/MC-CEM), describes the interaction energy of the ith atom A_i, within a set of N atoms as

$$\Delta E_i = \sum \Delta F_J(A_i, n_i) + \frac{1}{2} \sum_i \sum_j V_C(A_i, A_j). \qquad (1)$$

In this expression, n_i is the total electron ("jellium") density at the position of the ith atom which is calculated explicitly from the overlaps of atomic electron densities and $V_C(A_i, A_j)$ describes the coulombic interaction of nuclei and electrons of the atoms A_i and A_j which is calculated from first principles. The crucial quantity entering Eq. (1) is the empirical embedding function ΔF_J, which is obtained in a fairly complicated manner described in detail in Refs. 31 and 32. Briefly, the construction of ΔF_J utilizes two different sets of experimental data. In the region of high jellium density, ΔF_J is fit to the properties (i.e., the equilibrium cohesive energy and the bulk modulus) of the bulk solid. In the region of low jellium density, on the other hand, ΔF_J is obtained by inverting the binding energy curve of an isolated dimer, which, in turn, was parametrized as a Morse potential fit to known spectroscopic constants (i.e., dissociation energy, equilibrium interatomic distance, and vibration frequency). The final embedding function was then constructed by smoothly joining the two curves in the intermediate region.[32] MD/MC-CEM potentials designed this way have recently been used in MD simulations of the keV particle bombardment of Ni(001), Rh(001), and Au(111) surfaces, where the calculated energy resolved polar angle distributions of sputtered monomers were found to compare favorably with corresponding experimental data.[33,34] In the context of the present investigation, the great advantage of this potential is that the binding energy of small clusters is reproduced much more realistically than by the embedded atom method (EAM) potential which was used in our previous work (see below). In addition, the MD/MC-CEM potential can be directly employed for sputtering calculations, whereas the original EAM potential had to be modified to include a sufficiently repulsive interaction at small internuclear separations.[11,35] In the present study, we use a potential fit to the data of solid silver[36] and of the Ag_2 dimer.[37] The reason for choosing this particular potential was to compare some of the results obtained from the simulation to a relatively large set of experimental data available on the sputtering of neutral Ag_n clusters by keV Ar^+-bombardment of silver surfaces.[27]

The identification and classification of sputtered clusters was done in the same way as described in detail in Ref. 12. Briefly, the trajectory integration of the collision cascade initiated by the impinging primary particle was terminated at a time when the total energy of all atoms within the model crystal had fallen below a predefined threshold value of E_{th}=0.5 eV. At the highest primary ion energy of 5 keV, about 25% of the calculated trajectories did not reach this condition before being stopped at a maximum integration time limit of 1000 fs, for lower bombarding energies this fraction was much lower. Upon termination, the list of ejected atoms obtained for a given primary ion impact was examined for agglomerates of two or more atoms, the total (i.e., the sum of potential and relative kinetic) energy of which was detected to be negative. These so-called "nascent clusters" consisting of n atoms were then subjected to a stability check by evaluating their total internal energy and comparing it to the dissociation energy E_d, i.e., the lowest energy threshold

$$E_{th}^{(m)} = E_a(n-m) + E_a(m) - E_a(n) \qquad (2)$$

for unimolecular decomposition reactions given by

$$M_n \xrightarrow{E_{th}^{(m)}} M_{n-m} + M_m \quad (m = 1, \ldots, n-1).$$

The cluster atomization energies E_a as given by the MD/MC-CEM potential were determined as follows. Starting from an arbitrary configuration of n atoms which ensured that the total energy of the cluster was negative, the motion of the atoms was followed by MD while simultaneously removing energy from the system by a generalized Langevin algorithm[38] until the system eventually reached a frozen configuration corresponding to a local minimum of the potential surface. Then, the same algorithm was used to heat the cluster to temperatures of several thousand K, where the atom positions moved significantly and, hence, no defined cluster geometry was present any more. After an equilibration time of several picoseconds, the cluster was cooled down again and another, generally different local potential minimum was reached. This sequence of alternating heating and cooling cycles was repeated many times until the global potential minimum corresponding to the geometric ground state configuration of the cluster could be safely identified.

Nascent clusters with internal energies above the dissociation threshold were considered to be unstable and therefore subject to dissociation. The unimolecular fragmentation of these clusters during their path away from the surface was followed by further MD simulation using the same interaction potential as in the sputtering calculation but omitting all atoms except those in the nascent cluster in order to reduce the computation time. For simplicity of the calculation, the center-of-mass kinetic energy of the cluster was removed prior to the simulation, but the internal positions and velocities of the atoms in the cluster at the time the sputtering calculation was terminated were preserved. The trajectory integration was carried on until only stable fragments remained. These so-called "final" clusters are of particular interest, since they represent the only sputtered species which can be detected by experiment. In very few cases, particularly for unstable trimers with very low excess internal energy above the dissociation limit, a time limit of 500 ps was reached before fragmentation occurred. The number of these metastable clusters, however, was so small that their influence on the calculated properties of sputtered clusters can safely be neglected.

TABLE I. Calculated total sputtering yield Y_{tot} vs the primary ion energy for bombardment of an (111) silver single crystal surface with Ar^+ ions under normal incidence. Experimental data taken from Ref. 39.

	MD-Simulation	Expt.
5 keV	10.5	12.8
3 keV	11.7	11.4
1 keV	5.3	5.6
500 eV	3.9	...
250 eV	2.5	...

The simulations were performed for Ar^+ ions normally incident onto a silver (111) surface. Most of the calculations were done with a primary ion energy E_B of 5 keV. In order to facilitate enough statistics to reveal properties like kinetic and internal energy distributions of final clusters, a total of 4500 trajectories (equal to primary ion impacts) were run for these conditions. In order to ensure that the limited size of the model crystal does not falsify the simulation results, some selected trajectories which resulted in very high atomic and cluster emission yields were rerun with a larger crystal containing approximately 10 000 atoms and no significant changes were detected. The role of E_B with respect to the formation of sputtered clusters was investigated by additional simulations employing various different values of E_B between 250 and 5 keV. A total of 1000 trajectories were run for each of these simulations. In all cases, the impact points were chosen to be uniformly distributed over the smallest irreducible surface cell.

III. RESULTS AND DISCUSSION

Table I depicts the total sputtering yield Y_{tot} produced by the simulations in comparison with corresponding experimental data.[39] It is seen that both the magnitude as well as the bombarding energy dependence of Y_{tot} are well reproduced, a finding which may provide a first quality check of the interaction potential used.

Following the schedule outlined above, the remainder of Sec. III is organized into three different subsections. First, the properties of small silver clusters containing up to 10 atoms as predicted by the MD/MC-CEM potential are evaluated and compared to corresponding *ab initio* calculations and experimental data (where available). These results are of importance to judge the quality of the potential with respect to the description of small clusters. Then, the yields of sputtered nascent and final clusters as determined from the simulations are presented and compared to existing experimental data. The third subsection is devoted to the evaluation of energetic properties like translational energy distributions and internal excitation of the sputtered clusters.

A. Cluster properties

Figure 1 shows the binding energy per constituent atom of small silver clusters which is calculated from the MD/MC-CEM potential. The atomization energies E_a entering Eq. (2) are obtained by multiplicating these data with the number of atoms in the cluster. The resulting values of the

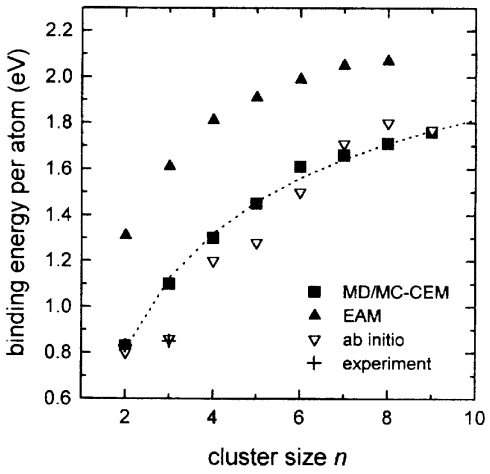

FIG. 1. Binding energy per atom of Ag_n clusters as calculated from the MD/MC-CEM potential. For comparison, literature data taken from recent *ab initio* calculations, (Ref. 41) experimental data, (Ref. 42) as well as the results obtained with the EAM potential are included.

fragmentation threshold energies are presented in Table II. It is found that practically in all cases the energetically favored fragmentation path predicted by the MD/MC-CEM potential is by evaporation of a monomer, a behavior which appears to be typical for transition metal clusters.[40] With the exception of Ag_4, the dissociation threshold E_d is therefore identical with the values given in the first row of Table II. For comparison, the results of recent *ab initio* calculations performed for the same clusters[41] as well as corresponding experimental data collected for silver dimers and trimers[42] are also included in Fig. 1. It is seen the CEM-results agree within less than 10% with the *ab initio* data, the only exception being the trimer, where the binding energy is overestimated by approximately 30%. Since the agreement is expected to improve with increasing cluster size, we therefore conclude that the CEM potential used here provides an excellent description of the bond energy of silver clusters. As is also seen from Fig. 1, this was not the case for the EAM potential used in our previous work, which is found to significantly overbind the small clusters. By comparing the data of Refs. 12 and 15 with the results presented in the following subsection, we are therefore now in position to examine the role the

TABLE II. Threshold energies $E_{th}^{(m)}$ for dissociation of Ag_n clusters into Ag_m and Ag_{n-m} fragments as evaluated from the MD/MC-CEM potential. Values are given in eV.

m	1	2	3	4	5
Ag_3	1.65				
Ag_4	1.91	1.90			
Ag_5	2.03	2.28			
Ag_6	2.31	2.68	2.94		
Ag_7	2.06	2.71	3.09		
Ag_8	2.09	2.49	3.15	3.27	
Ag_9	2.11	2.54	2.95	3.35	
Ag_{10}	2.21	2.66	3.10	3.25	3.53

cluster "overboundedness" plays in predicting the yields and energy distributions of sputtered clusters.

The geometric equilibrium configurations of the clusters which correspond to the detected energetic ground state are the same as those presented in Ref. 31 for Ni_n clusters (which were also determined using an MD/MC-CEM potential). They are also identical with those obtained for Ag_n clusters using the EAM potential[12] and are therefore presumably typical for a spherically symmetric interaction potential. Not in all cases, however, the structure predicted here coincides with that determined *ab initio*: In Ref. 41, the trimer is found to be Jahn–Teller distorted from the equilateral triangle, and the ground state configuration of the tetramer is flat instead of tetrahedral. The structures of Ag_7 and Ag_8 are the same as those obtained here, and for Ag_5 and Ag_6 the energetic differences between the ground state and the structure predicted by the MD/MC-CEM potential are 0.003 and 0.31 eV, respectively.

With regard to the extension towards larger clusters (Sec. III B), we wish to extrapolate the CEM-binding energies to clusters containing more than ten atoms. For these species, the MD method outlined in Sec. II is not practicable, since the number of local potential minima corresponding to metastable cluster states rapidly increases with increasing number of constituent atoms. We therefore chose to extrapolate the data of Fig. 1 by means of a simple functional form

$$E_a(n) \cong n U_s (1 - c n^{-\kappa}), \tag{3}$$

which corresponds to a modified liquid drop model of the clusters. In Eq. (3), U_s denotes the sublimation energy of the solid metal [note that the CEM potential was fit to reproduce the respective value (3.0 eV) of silver], and the parameter c is related to the surface tension of the cluster. Strictly speaking, the exponent should be fixed to $\kappa = 1/3$, if Eq. (3) is justified in terms of a liquid drop model. In order to obtain a better fit to the data of Fig. 1, however, we chose to regard both c and κ as fitting parameters yielding $c = 0.95$ and $\kappa = 0.38$, respectively. The resulting curve has been included in Fig. 1.

B. Cluster yields

Figure 2 shows the relative yield, i.e., the partial yield normalized to that of the monomers, of sputtered nascent clusters as a function of the cluster size. For comparison, the results of MD simulations performed for two different primary ion energies are shown. It is seen that the yield distributions can be accurately described by a power law according to

$$Y_{\text{nasc}}(n) \propto n^{-\alpha}, \tag{4}$$

with exponents α which increase with decreasing primary ion energy. The same behavior was also found in our previous calculations using the EAM potential[15] and therefore seems to be rather typical for nascent sputtered metal clusters. As shown in Table III, however, the absolute values of α predicted by the EAM potential are significantly lower than those evaluated here, i.e., the EAM results largely overestimate the contribution of larger clusters to the total flux of sputtered particles. As already pointed out in Ref. 12, this finding is not surprising due to the fact that the EAM potential overbinds the clusters and, hence, renders more candidate aggregates of atoms with negative total energy than the CEM potential.

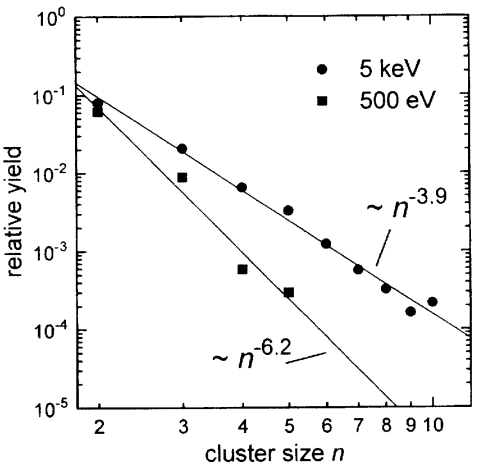

FIG. 2. Relative yields (i.e., yields normalized to that of monomers) of nascent clusters produced upon impact of normally incident Ar^+ ions onto an Ag(111) surface vs the cluster size for two different values of the primary ion energy.

In order to proceed, it is necessary to investigate the sputtered nascent clusters with respect to their total internal energy. As described in Sec. III C, we find broad distributions which result in a linear increase of the average internal energy with increasing cluster size according to

$$E_{\text{int}}^{\text{av}}(n) \cong (1.40n - 1.86) \text{ eV}, \tag{5}$$

as displayed in Fig. 3. This finding as well as the numerical values in Eq. (5) are almost identical with the EAM results,[12] thus indicating that the average internal energy of sputtered nascent clusters is characteristic for the collision sequences leading to the ejection of the constituent atoms rather than for the binding energy of the cluster. As also seen from Fig. 3, the average internal energy of nascent clusters does not depend on the bombarding energy E_B. This is important since it shows that relation (5) evolves as a result of the sputtering process instead of merely reflecting the sharing of the primary ion energy among all atoms of the model crystallite.

TABLE III. Power law exponent α of the yield distribution of sputtered nascent clusters [Eq. (4)] as calculated from the MD simulation results. For comparison, the corresponding values predicted in Ref. 15 using the EAM potential are also given.

	MD/MC-CEM	EAM (Ref. 15)
5 keV	3.9	2.9
3 keV	4.0	...
1 keV	5.0	4.7
500 eV	6.2	5.5
250 eV	9.3	7.1

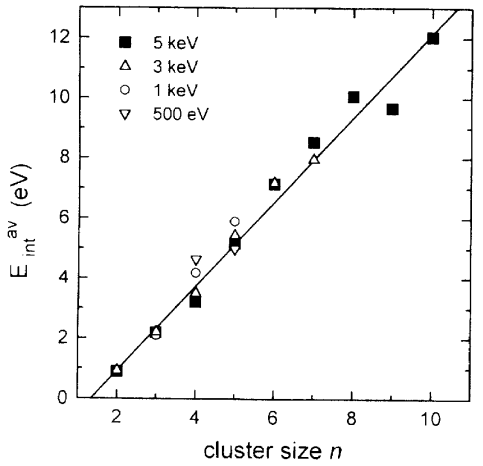

FIG. 3. Average internal energy of nascent Ag_n clusters produced upon impact of normally incident Ar^+ ions of various kinetic energies onto an Ag(111) surface. Straight line: least square fit according to Eq. (5) in the text.

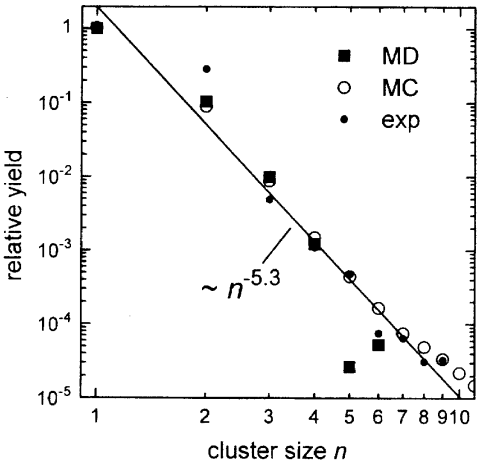

FIG. 4. Relative yields (i.e., yields normalized to that of the monomers) of final clusters produced upon impact of normally incident 5-keV Ar^+ ions onto an Ag(111) surface. MD: results of molecular dynamics simulation alone; MC: results of model calculation combining Molecular Dynamics and Monte Carlo simulation as described in the text; exp: experimental data taken from Ref. 27. Solid line: least square apparent linear fit to the calculated data termed MC.

Using the calculated internal energy distribution in connection with the dissociation thresholds evaluated above, we can define a survival probability $P_{surv}(n)$ of nascent clusters as that fraction which contains less internal energy than necessary for dissociation. We find $P_{surv}(3)=0.21$, $P_{surv}(4)=0.05$, and $P_{surv}(n\geq 5)=0$. This implies that about 80% of the nascent trimers, 95% of the tetramers, and virtually all of the nascent clusters containing 5 or more atoms are unstable and will therefore fragment on their path away from the surface. Since we have the positions and momenta of the individual constituent atoms, we can follow the fragmentation by further MD simulation until—in the ideal case—only stable fragments remain. In accordance with the EAM results, we find that the vast majority of the unimolecular decomposition reactions occur on a subpicosecond or at most picosecond time scale. The nascent clusters defined above must therefore be regarded as transient stages during particle emission, the properties of which will quickly evolve in time. It should be noted that the data of Figs. 2 and 3 represent momentary snapshots of this evolution which depend on the particular moment at which the MD trajectory integration is stopped (and thus implicitly on the choice of the threshold energy value E_{th} introduced in Sec. II). Although the definition and identification of nascent clusters is therefore not entirely unambiguous, we feel that it is these species which carry most of the information on the collisional cluster formation processes in sputtering.

Among about 1000 unstable trimers (nascent or fragmentation products), only 5 containing extremely low excess internal energy above the dissociation limit reached the integration time limit of 500 ps before dissociating. For tetramers, the percentage of these metastable clusters was even less, and no such event occurred for larger unstable clusters. Since, on the other hand, there is much experimental evidence for the generation of larger metastable clusters in sputtering,[43,44] this only means that their yields must be very small and therefore fall below the limit imposed by the statistics of the present calculation. Hence, we can safely neglect the role of metastable species in evaluating the yield distribution of "final," i.e., stable clusters which remain at the end of the fragmentation chains. Due to the short dissociation lifetime, practically only these particles are experimentally detected as "sputtered clusters." Figure 4 shows the results for $E_B=5$ keV. It is seen that the relative yield of final clusters drops significantly faster than that of the nascent clusters, the largest final cluster detected in the MD simulation being a hexamer. For comparison, recent experimental data[27] on the yield distribution of Ag_n clusters sputtered from a polycrystalline silver surface by 5-keV Ar^+ ions are included in the figure. It is apparent that at least up to Ag_4 the MD results calculated using the CEM potential provide an almost quantitative description of the experimental cluster yields, a finding which is in marked contrast to the results obtained using the EAM potential. This confirms our earlier conclusion that the overestimation of final cluster yields which was found with the EAM potential was due to its overbinding of the clusters. For Ag_5 and Ag_6, the total numbers of clusters detected in the simulation (1 and 2, respectively) are obviously too low to make a conclusive statement.

In order to extend the prediction of cluster yields to larger clusters as well, we apply a simple statistical model calculation which has been described in great detail earlier.[15] Briefly, the yield distribution of nascent clusters as given by the MD simulations is extrapolated to larger aggregates by means of Eq. (4). In a Monte-Carlo approach, the unimolecular fragmentation of nascent clusters into stable products is then followed using statistical Rice–Ramsperger–Kassel (RRK) rate theory[45] by assuming that each nascent cluster contains a fixed internal energy as given by Eq. (5). As shown in Ref. 15, this leads to fragmentation patterns which are in good agreement with the MD data. The resulting dis-

TABLE IV. Power law exponent δ of the yield distribution of sputtered final clusters [Eq. (6)] as calculated from the Monte Carlo model described in the text for various values of the primary ion energy E_B. For comparison, the corresponding experimental data taken from Ref. 27 have been included.

	Model calculation	Expt.
5 keV	4.6	5.3
3 keV	4.8	5.8
1 keV	6.0	7.3
500 eV	7.5	...
250 eV	11.4	...

TABLE V. Bound state fraction f_{bound}, i.e., fraction of sputtered atoms which are detected as part of a final cluster, for bombardment of an Ag(111) surface with normally incident Ar^+ ions of different energies. Experimental data taken from Ref. 27. Values are given in percent.

	MD-Simulation	Expt.
5 keV	19.6	37.3
3 keV	18.9	32.9
1 keV	12.4	24.0
500 eV	12.6	...
250 eV	7.1	...

tribution of final cluster yields is also included in Fig. 4. First, it is seen that for $n \leqslant 4$ the model calculation agrees well with the original MD results and, hence, provides an essentially correct description of the fragmentation processes. Second, we find that only for the case of dimers the deviation between calculated and measured cluster yield slightly exceeds a factor of 2. In view of the large yield variation by roughly four orders of magnitude, we consider this a very good reproduction of the experimental cluster size distributions. This finding is of special importance, since to our knowledge no alternative model exists to date which is capable to describe the power law yield distributions which have been determined experimentally for a variety of different ion-target systems[46,47] and must therefore be regarded as a general feature of metal cluster sputtering. If we fit a power law

$$Y_{\text{final}}(n) \propto n^{-\delta} \tag{6}$$

to the yield distributions calculated here, we obtain exponents δ which are listed in Table IV together with the corresponding values extracted from experimental data.[27] It is evident that the strong dependence of the yield distribution on experimental parameters like the nature or energy of the impinging primary ion which is observed experimentally is clearly reproduced by the simulation. Interestingly, comparing the values of Tables III and IV, one finds a constant ratio of 1.2 between the exponents δ and α. Although the numerical value was somewhat different (1.3), this was also observed in our earlier EAM study and therefore seems to be a rather general result. The physical origin of this correlation is unclear at the present time. It can, however, provide a means to gain information on the yield distribution of sputtered nascent clusters which is otherwise unaccessible by experiment.

From the data of Fig. 4, the total fraction f_{bound} of sputtered atoms which are detected as part of a final cluster can be determined. The results are depicted in Table V for different values of the primary ion energy. It is seen that f_{bound} decreases with decreasing E_B, a trend which is in accordance with the experiment.[27] However, the calculated values of f_{bound} are about a factor of 2 lower than the experimental values which are also displayed in Table V.

C. Energy distributions

The kinetic, i.e., center-of-mass energy distributions of final clusters as evaluated from the MD simulation at $E_B = 5$ keV are shown in Fig. 5. Comparison with the corresponding experimental data reveals agreement in the region above 2 eV but deficiencies of low energy clusters in the calculation. Whether this discrepancy is due to problems with the simulation or with the experiment is not clear at the present time. We note, however, that the distributions calculated here are in close agreement with our previous results[11] (dimers only) as well as with those calculated by Betz and Husinsky[17] for sputtered Cu_n clusters, both of which were obtained using an EAM interaction potential.

A point of great interest concerns the internal energy of sputtered clusters. Corresponding data for nascent clusters has already been presented in Fig. 3. Assuming a thermal distribution of excited states, relation (5) can be converted into internal temperatures T_{int}. Since the average energy contained in a vibrational and rotational degree of freedom amounts to kT_{int} and $(1/2)kT_{\text{int}}$, respectively, for nonlinear clusters larger than dimers, the internal energy is to a first order approximation given by

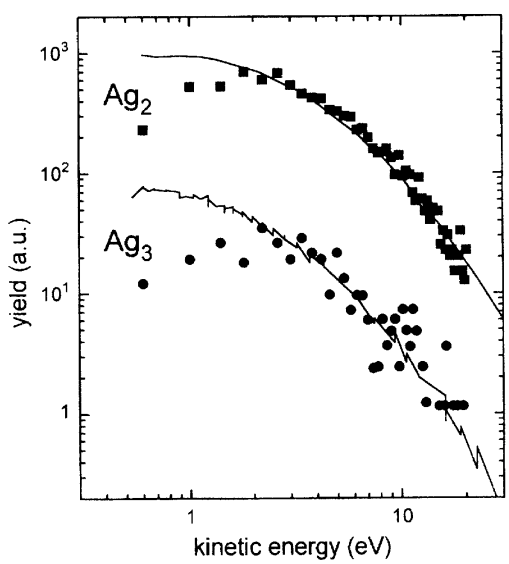

FIG. 5. Kinetic energy distributions of final clusters produced upon impact of normally incident 5-keV Ar^+ ions onto an Ag(111) surface. Solid lines: experimental data taken from Ref. 27.

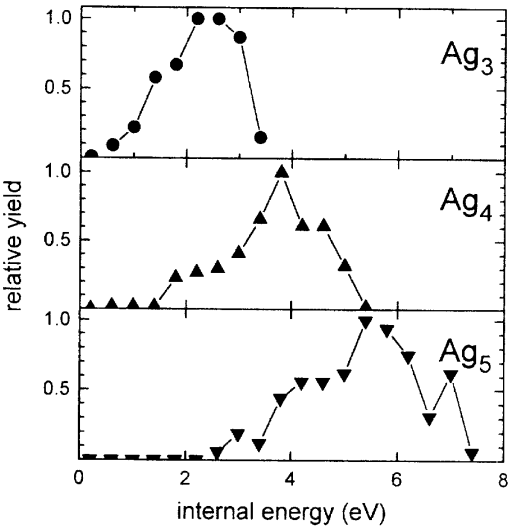

FIG. 6. Internal energy distribution of nascent clusters produced upon impact of normally incident 5-keV Ar^+ ions onto an Ag(111) surface.

$$E_{\text{int}}(n)=[(3n-6)+\tfrac{3}{2}]kT_{\text{int}}. \quad (7)$$

Note the similarity between Eqs. (5) and (7), which indicates an internal temperature of $T_{\text{int}} \sim 5400$ K regardless of the cluster size. Figure 6 shows the related internal energy distributions of nascent clusters. Unfortunately, an experimental verification of these data appears to be extremely difficult if not impossible. Figure 7 therefore shows the calculated internal energy distribution of final dimers, trimers, and tetramers which can in principle be compared to experimental data. As expected, the distributions fill the complete interval between zero and the dissociation limit, thus indicating that many rovibrational states of the clusters are populated. For the case of dimers, we can explicitly calculate the population of rotational and vibrational levels by a straightforward quantization scheme described in detail in Ref. 11. The resulting rovibrational distribution of sputtered silver dimers is shown in Figs. 8 and 9. In order to improve the statistics,

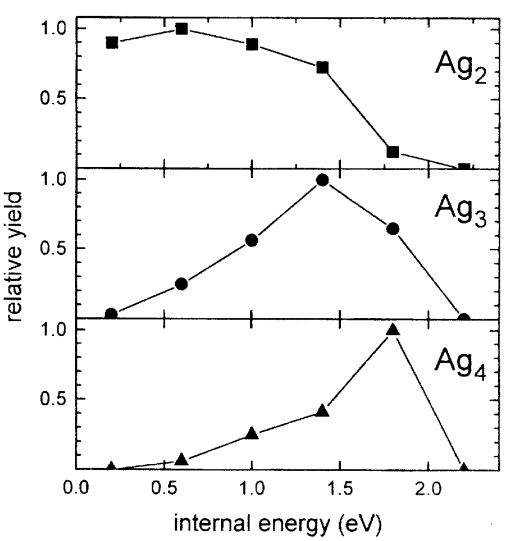

FIG. 7. Internal energy distribution of final clusters produced upon impact of normally incident 5-keV Ar^+ ions onto an Ag(111) surface.

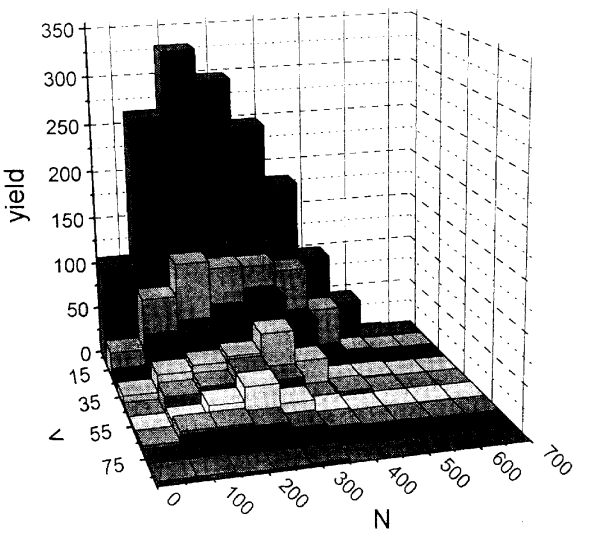

FIG. 8. Ro-vibrational population of dimers (nascent and fragmentation products) produced upon impact of normally incident 5-keV Ar^+ ions onto an Ag(111) surface. The data have been histogrammed into slots of 10 and 70 vibrational and rotational quantum numbers v and N, respectively, in order to reduce the statistical noise.

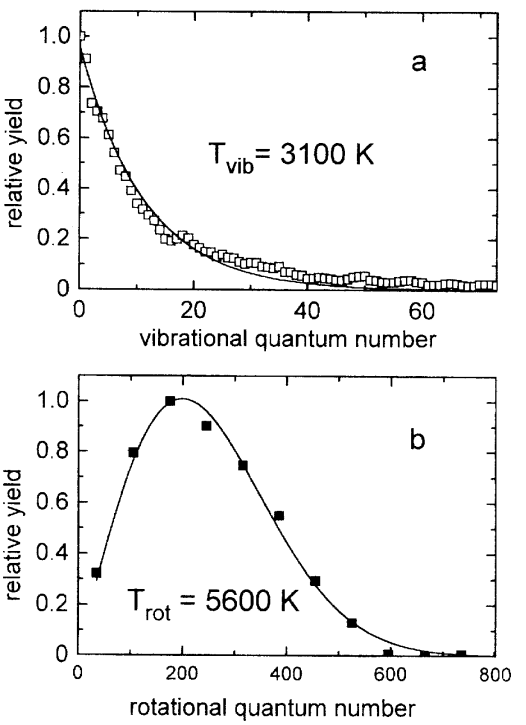

FIG. 9. Rotationally integrated vibrational (a) and vibrationally resolved ($0 \leq v \leq 10$) rotational (b) population distribution of Ag_2 dimers (nascent and fragmentation products) detected upon impact of normally incident 5-keV Ar^+ ions onto an Ag(111) surface. Solid lines: Boltzmann fits using the indicated population temperatures and spectroscopical constants of the ground state silver dimer taken from Ref. 50.

the data in Fig. 8 have been histogrammed into slots of 10 and 70 vibrational and rotational quantum numbers v and N, respectively. In Fig. 9(a), each data point was evaluated by adjacent averaging of the rotationally integrated population between $v-1$ and $v+1$, whereas the data of Fig. 9(b) corresponds to the first row of Fig. 8 ($0 \leq v \leq 10$). [The reason for not averaging the distribution of Fig. 9(b) over all vibrational quantum numbers is that the rotational distribution is expected to change with increasing vibrational excitation: at high v the N-distribution must necessarily be cut off at high N due to the dissociation limit of the molecule.] It is seen that the population of both vibrational and rotational states can be very accurately approximated by quasi-thermal, i.e., Boltzmannlike distributions with, however, different rotational and vibrational temperatures T_{rot} and T_{vib}, respectively. From the data depicted in Fig. 9, we find $T_{\mathrm{rot}}=5900$ K and $T_{\mathrm{vib}}=3100$ K in close agreement with our previous EAM data.[11,13] A closer look reveals that T_{rot} exhibits a slight increase with increasing vibrational quantum numbers, the effect, however being fairly small (<30%) and at high v numbers of course limited by the dissociation threshold of the molecule. We note that the population temperatures determined here are in very good agreement with corresponding experimental data[48] yielding values of $T_{\mathrm{rot}}=6700$ K and $T_{\mathrm{vib}}=2700$ K. We note also that, although dimers *a priori* cannot undergo unimolecular fragmentation reactions as described above, the dissociation of larger clusters may significantly contribute to the total distribution of dimers detected far away from the surface. In the example of Fig. 8, for instance, 25% of the total dimers are constituted by fragmentation products which, in turn, exhibit significantly lower internal temperatures ($T_{\mathrm{rot}}=2700$ K, $T_{\mathrm{vib}}=1900$ K) than the nascent dimers ($T_{\mathrm{rot}}=7400$ K, $T_{\mathrm{vib}}=4100$ K).

For the larger clusters, the spectroscopy becomes exceedingly complicated, therefore, we did not attempt a detailed rovibrational analysis. It is apparent that with growing cluster size the role of rotation with regard to the total internal energy becomes negligibly small due to the rapidly increasing number of vibrational degrees of freedom. An experimental verification of the energy distributions depicted in Fig. 7, although in principle feasible, is still lacking. Data on sputtered neutral Ag_4, Ag_6, and Ag_8, although of somewhat preliminary nature, indicate that an abundant fraction of the detected clusters possess internal energies in excess of 0.25, 0.75, and 0.7 eV, respectively,[48] a finding which is consistent with the results presented in Fig. 7. We like to stress again that experimental detection schemes basically provide information on final clusters. In principle, it would be of great interest to determine the time evolution of the mass and internal energy distribution of sputtered clusters as they move away from the surface. At least the late stages of the unimolecular fragmentation chains might be tractable, since, as discussed above, a small fraction of the clusters will at some time become metastable on time scales larger than that studied here. In a series of experiments, Dzhemilev and co-workers[28] have investigated the unimolecular fragmentation of sputtered ionic metal clusters (Ta_n^+ and Nb_n^+) on time scales ranging down to the nanosecond range. Unfortunately, in our simulation practically all of the clusters containing more than 4 atoms have completely decomposed into stable products before that time, and therefore, presumably due to statistical limitations, no overlap between the experimental data and the MD simulation exists. However, by extrapolation of the measured fragmentation rate data towards the picosecond time range, the authors of Ref. 28 claim to have verified our prediction of an internal energy of the order of 1 eV per constituent atom within nascent clusters.[49]

IV. CONCLUSION

We have used a new many-body interaction potential (MD/MC-CEM) to simulate the formation of clusters during sputtering of solid silver by molecular dynamics. It is shown that the MD/MC-CEM potential, which is fit to properties of the target material in both solid and diatomic environments, allows a much more realistic description of small clusters than the EAM potential used in our previous investigations. As a consequence, the significant overestimation of cluster yields which had been observed earlier is removed in the present calculations, and the contribution of clusters to the total flux of sputtered material can now be described in almost quantitative agreement with experimental data. The predictions with respect to kinetic and internal energy distributions of sputtered clusters are not very different from to those obtained with the EAM potential, suggesting that the energetic properties of sputtered clusters are less affected by the absolute well depth. Interestingly, for all nascent clusters regardless of size we find internal temperatures around 5400 K, which rapidly decrease by evaporative cooling mechanisms as the clusters move away from the surface, until at times of the order of picoseconds after the emission practically only stable fragments remain. In all cases where calculated properties are compared to corresponding experimental data, we find agreement on an at least semiquantitative level. In our opinion, this result is the more impressing since the experimental data were exclusively collected on polycrystalline targets, whereas the MD simulation naturally refers to a perfect single crystal (111) surface. Keeping this in mind, we arrive at the conclusion that molecular dynamics simulation in combination with the modern many-body potentials which are now available provides an excitingly accurate tool to describe the formation of clusters in sputtering of metallic surfaces.

ACKNOWLEDGMENTS

The authors would like to thank A. E. DePristo for making the MD/MC-CEM potential available to us. B.J.G. acknowledges the financial support of the National Science Foundation and the IBM Selected University Research Program.

[1] H. M. Urbassek and W. O. Hofer, Det kongelige Danske Vid. Selsk. Mat. Fys. Medd. **43**, 97 (1993).
[2] D. E. Harrison, Jr. and C. B. Delaplain, J. Appl. Phys. **47**, 2252 (1976).
[3] N. Winograd, D. E. Harrison, Jr., and B. J. Garrison, Surf. Sci. **78**, 467 (1978).

[4] B. J. Garrison, N. Winograd, and D. E. Harrison, Jr., J. Chem. Phys. **69**, 1440 (1978).
[5] B. J. Garrison, N. Winograd, and D. E. Harrison, Jr., Phys. Rev. B **18**, 6000 (1978).
[6] N. Winograd, K. E. Foley, B. J. Garrison, and D. E. Harrison, Jr., Phys. Lett. A **73**, 253 (1979).
[7] N. Winograd, B. J. Garrison, T. Fleisch, W. N. Delgass, and D. E. Harrison, Jr., J. Vac. Sci. Technol. **16**, 629 (1979).
[8] S. P. Holland, B. J. Garrison, and N. Winograd, Phys. Rev. Lett. **44**, 756 (1980).
[9] B. J. Garrison, J. Am. Chem. Soc. **102**, 6553 (1980).
[10] D. E. Harrison, Jr., P. Avouris, and R. Walkup, Nucl. Instrum. Methods B **18**, 321 (1987).
[11] A. Wucher and B. J. Garrison, Surf. Sci. **260**, 257 (1992).
[12] A. Wucher and B. J. Garrison, Phys. Rev. B **46**, 4855 (1992).
[13] F. Karetta and H. M. Urbassek, Appl. Phys. A **55**, 364 (1992).
[14] A. Wucher and B. J. Garrison: Nucl. Instrum. Methods B **82**, 352 (1993).
[15] G. Betz, R. Kirchner, W. Husinsky, F. Rüdenauer, and H. M. Urbassek, Radiat. Eff. **130/131**, 251 (1994).
[16] A. Wucher, Nucl. Instrum. Methods B **83**, 79 (1993).
[17] M. H. Shapiro and T. A. Tombrello, Nucl. Instrum. Methods B **84**, 453 (1994).
[18] Y. Yamamura, *Secondary Ion Mass Spectrometry SIMS IX*, edited by A. Benninghoven, Y. Nihei, R. Shimizu, and H. W. Werner (Wiley, Chichester, 1994), p. 3
[19] H. Gades and H. M. Urbassek, Nucl. Instrum. Methods B **103**, 131 (1995).
[20] G. Betz, R. Kirchner, G. Nicolussi, and W. Husinsky: *Secondary Ion Mass Spectrometry SIMS IX*, edited by A. Benninghoven, Y. Nihei, R. Shimizu, and H. W. Werner (Wiley, Chichester, 1994), p. 57
[21] M. H. Shapiro, K. R. Bengtson, and T. A. Tombrello, Nucl. Instrum. Methods B **103** 123 (1995).
[22] G. Betz and W. Husinsky, Nucl. Instrum. Methods B **102**, 281 (1995).
[23] S. M. Foiles, M. I. Baskes, and M. S. Daw, Phys. Rev. B **33**, 7983 (1986).
[24] S. R. Coon, W. F. Calaway, J. W. Burnett, M. J. Pellin, D. M. Gruen, D. R. Spiegel, and J. M. White, Surf. Sci. **259**, 275 (1991).
[25] A. Wucher, M. Wahl, and H. Oechsner, Nucl. Instrum. Methods B **82**, 337 (1993).
[26] S. R. Coon, W. F. Calaway, M. J. Pellin, and J. M. White, Surf. Sci. **298**, 161 (1993).
[27] M. Wahl and A. Wucher, Nucl. Instrum. Methods B **94**, 36 (1994).
[28] N. Kh Dzhemilev, A. M. Goldenberg, I. V. Veriovkin, and S. V. Verkhoturov, Int. J. Mass. Spectrom. Ion. Proc. **141**, 209 (1995) and references therein.
[29] T. J Raeker and A. E. DePristo, Int. Rev. Phys. Chem. **10**, 1 (1991).
[30] D. E. Harrison, Jr., Crit. Rev. Solid State Mater. Sci. **14**, 51 (1988).
[31] M. S. Stave, D. E. Sanders, T. J. Raeker, and A. E. DePristo, J. Chem. Phys. **93**, 4413 (1990).
[32] C. L. Kelchner, D. M. Halstead, L. S. Perkins, N. M. Wallace, and A. E. DePristo, Surf. Sci. **310**, 425 (1994).
[33] S. W. Rosencrance, J. S. Burnham, D. E. Sanders, C. He, B. J. Garrison, and N. Winograd, Phys. Rev. B **52**, 6006 (1995).
[34] S. W. Rosencrance, N. Winograd, B. J. Garrison, and Z. Postawa: Phys. Rev. B **53**, 2378 (1996).
[35] B. J. Garrison, N. Winograd, D. M. Deaven, C. T. Reimann, D. Y. Lo, T. A. Tombrello, D. E. Harrison, Jr., and M. H. Shapiro, Phys. Rev. B **37**, 7197 (1988).
[36] Ch. Kittel: *Introduction to Solid State Physics* (Wiley, New York, 1971).
[37] M. D. Morse, Chem. Rev. **86**, 1049 (1986).
[38] B. J. Garrison, P. B. S. Kodali, and D. Srivastava, Chem. Rev. **96**, 1327 (1996).
[39] G. D. Magnuson and C. E. Carlston, J. Appl. Phys. **34**, 3267 (1963).
[40] M. F. Jarrold in *Clusters of Atoms and Molecules*, edited by H. Haberland (Springer, New York, 1994), p. 320.
[41] V. Bonacic-Koutecky, L. Cespiva, P. Fantucci, and J. Koutecky, J. Chem. Phys. **98**, 7981 (1993).
[42] K. Hilpert and K. A. Gingerich, Ber. Bunsenges. Phys. Chem. **84**, 739 (1980).
[43] W. Begemann, S. Dreihöfer, K. H. Meiwes-Broer, and H. O. Lutz, Z. Phys. D **3**, 183 (1986).
[44] N. Kh. Dzhemilev, A. M. Goldenberg, I. V. Veriovkin, and S. V. Verkhoturov, Int. J. Mass Spectrom. Ion. Proc. **141**, 209 (1995), and references therein.
[45] P. J. Robinson and K. A. Holbrook, *Unimolecular Reactions* (Wiley, London, 1972), p. 53.
[46] S. R. Coon, W. F. Calaway, M. J. Pellin, and J. M. White, Surf. Sci. **298**, 161 (1993).
[47] A. Wucher and M. Wahl, Nucl. Instrum. Methods B **115**, 581 (1996).
[48] A. Wucher, Phys. Rev. B **49**, 2012 (1994).
[49] I. V. Veriovkin, S. V. Verkhoturov, A. M. Goldenberg, and N. Kh. Dzhemilev, Izv. Akad. Nauk Ser. Fiz. **58**, 57 (1994), and private communication.
[50] V. Beutel, H. G. Krämer, G. L. Bhale, M. Kuhn, K. Weyers, and W. Demtröder, J. Chem. Phys. **98**, 2699 (1993).